IOPscience iopscience.iop.org

Home Search Collections Journals About Contact us My IOPscience

Sputter Deposition of Multi-Element Nanoparticles as Electrocatalysts for Methanol Oxidation

This content has been downloaded from IOPscience. Please scroll down to see the full text.

2008 Jpn. J. Appl. Phys. 47 5755

(http://iopscience.iop.org/1347-4065/47/7R/5755)

View the table of contents for this issue, or go to the journal homepage for more

Download details:

IP Address: 140.113.38.11
This content was downloaded on 25/04/2014 at 15:42

Please note that terms and conditions apply.

Japanese Journal of Applied Physics
Vol. 47, No. 7, 2008, pp. 5755–5761

©2008 The Japan Society of Applied Physics

Sputter Deposition of Multi-Element Nanoparticles as Electrocatalysts for Methanol Oxidation

Chih-Fang TSAI, Pu-Wei WU*, Pang LIN, Cheun-Guang CHAO, and Kung-Yu YEH

Department of Materials Science and Engineering, National Chiao Tung University, Hsinchu 30010, Taiwan, R.O.C.

(Received October 31, 2007; revised February 25, 2008; accepted March 28, 2008; published online July 11, 2008)

Fabrication of multi-element nanoparticles on noncatalyzed gas diffusion electrodes (GDEs) by radio frequency sputter deposition was reported. X-ray diffraction analysis of the as-deposited films indicated crystalline fcc phases while energy dispersive X-ray spectroscope confirmed their composition as $Pt_{50}Fe_{11}Co_{10}Ni_{11}Cu_{10}Ag_8$. Scanning electron microscopy images revealed nanoparticulate nodules growing on the carbon particles. Cyclic voltammetry (CV) was employed to analyze their methanol oxidation abilities for direct methanol fuel cells. The CV responses improved upon cycling and became stabilized after 70 cycles. The areas under the CV curves were proportional to the amount of nanoparticles deposited. In mass activities the GDE with 5 nm nanoparticles demonstrated the highest values of 400–600 mA/mg. In comparing with Pt and $Pt_{43}Ru_{57}$, the $Pt_{43}Ru_{57}$ exhibited the lowest onset potential with the highest mass activities. Our work presents preliminary information on the catalytic behaviors of multi-element nanoparticles which is likely to bring new directions in catalyst design. [DOI: 10.1143/JJAP.47.5755]

KEYWORDS: multi-element alloy, sputter deposition, electrocatalyst, direct methanol fuel cell, nanoparticle

1. Introduction

Researches on direct methanol fuel cells (DMFC) have attracted considerable attentions for their promising potentials as the power source for portable electronics and transportation applications.[1,2] Since the methanol oxidation is intrinsically slow, one of the critical issues to improve the power density of DMFC is the development of effective anode electrocatalysts.[3] Because of acidic electrolyte involved, electrocatalytic materials must be corrosion-resistant. The Pt was explored for its respectable chemical inertness. Unfortunately, due to the CO adsorption after methanol dehydrogenation additional element is required to promote subsequent CO oxidation into CO_2. Strategies in alloying the Pt with secondary elements are rationalized by mechanisms including bifunctional effect and ligand model.[4,5] Earlier developments have concentrated on binary Pt based alloys such as PtRu, PtFe, PtCo, as well as PtNi.[6–9] Among them, the PtRu demonstrates the highest performance. In addition, ternary and quaternary Pt-based alloys such as PtRuCo, PtRuOs, PtRuIrOs, PtRuNiZr, and PtRuRhNi have been investigated with moderate success.[10–14] To date, electrocatalysts with more than four constituent elements have not been reported yet because of difficulty in chemical synthesis.

Design of alloys with multiple principal elements at equimolar or near-equimolar ratios (e.g., $CuCoNiCrAl_xFe$, MoTiVFeNiZrCoCr) was recently proposed by Yeh *et al.*[15] Due to a substantial increase of mixing entropy, the formation of complex intermetallic compounds is largely subdued. Instead, a simple solid solution containing fine crystallites is obtained with impressive characteristics in mechanical strengths as well as resistances to wear, corrosion, and oxidation at high temperatures.[16–18] Generally, the preparation of multi-element alloys is carried out in conventional metallurgic methods where bulk materials are formed by melting and solidification. On the other hand, the synthesis of nanomaterials with multiple elements has not been investigated yet. It would be significant scientific interest to prepare multi-element nanoparticles and study their electrochemical performances.

A functional anode in DMFC is fabricated by impregnating suitable electrocatalysts on the gas diffusion electrodes (GDEs). Typical impregnation process entails wet chemical approaches where precursors of metal ions are reduced and deposited onto selective carbonaceous supports. Alternative route of physical vapor deposition like sputtering is also explored. For example, O'Hayre *et al.* adopted the sputter deposition to prepare a Pt thin layer (5–10 nm) on the surface of Nafion membrane and reported notable improvements in power output.[19] Similar results were documented by Haug *et al.* and Alvisi *et al.* in which significant enhancements were observed when a thin layer of Pt was deposited on the GDE surface.[20,21] Although established GDE fabrication techniques favor the chemical reduction method to produce desirable electrocatalysts, the implementation of sputter deposition enables us to prepare nanoparticles with multiple elements in a relatively simple step. It is because the synthesis of multi-element nanoparticles by the chemical reduction route is challenging, particularly when the redox potentials of individual constituents differ substantially. Previously, the sputter deposition was demonstrated to produce crystalline multi-element films.[22] Therefore, it is feasible to employ the sputter deposition to prepare multi-element nanoparticles for electrochemical studies.

In this work, we report the fabrication of Pt-based crystalline multi-element nanoparticles as the anode electrocatalyst for DMFC by radio frequency (RF) sputter deposition. Secondary elements selected are Fe, Co, Ni, Cu, and Ag. They were chosen because they are expected to form a fcc solid solution with the Pt and their individual catalytic effects in alloying with the Pt have been reported in literatures.[7–9,23,24] This research is our preliminary efforts to explore multi-element nanoparticles for their electrochemical behaviors in fuel cell applications.

2. Experimental Procedure

The fabrication of multi-element nanoparticles was carried out by the sputter deposition of a target material onto a noncatalyzed GDE ($4 \times 4\,cm^2$). For preparation of the

*E-mail address: ppwu@mail.nctu.edu.tw

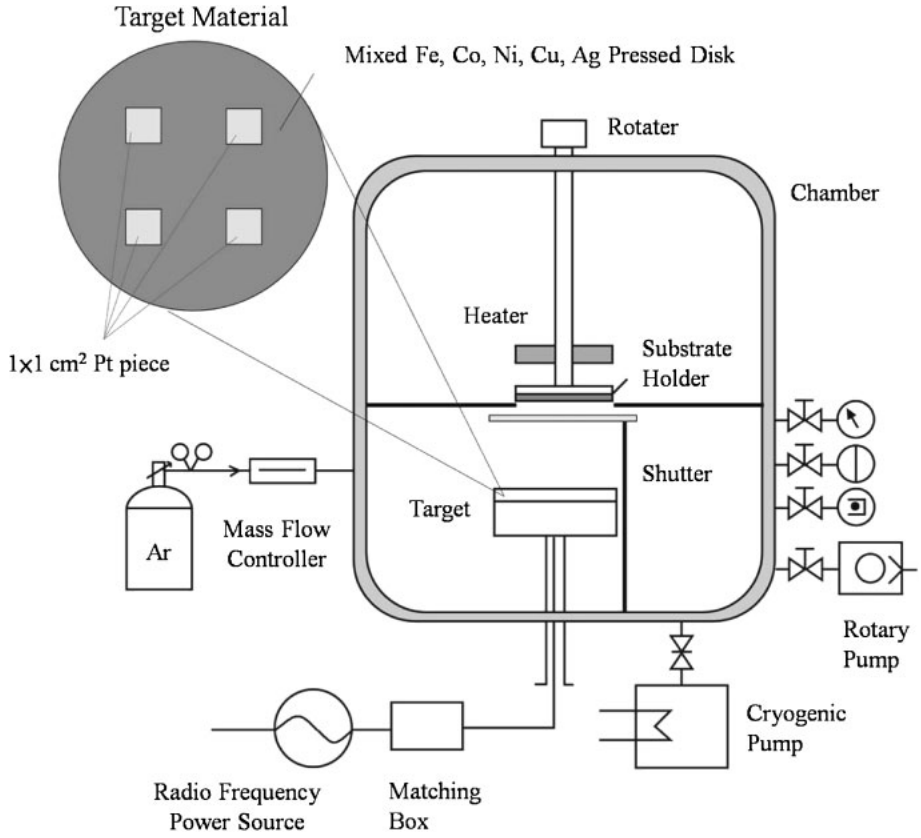

Fig. 1. A schematic of the sputter deposition setup.

noncatalyzed GDE, a dispersion of 70 wt % Shawinigan Acetylene Black (Chevron) and 30 wt % poly(tetrafluorethylene) (PTFE) was painted repeatedly onto a carbon cloth (E-TEK) to form a porous electrode followed by a heat treatment at 350 °C for 30 min in air. The resulting weight of the noncatalyzed GDE is 22 mg/cm^2. For the target material used during the sputter operation, metal powders of Co (1.4 μm in diameter), Ni (2.5 μm in diameter), Ag (0.8 μm in diameter), Cu (45.0 μm in diameter), and Fe (10.3 μm in diameter) were used. They were mixed and sealed with a polyethylene bottle in a nitrogen-filled glovebox at a molar ratio of 24 : 22 : 21 : 15 : 18 (Fe : Co : Ni : Cu : Ag). To ensure complete mixing, a dry tumbling was performed for 24 h with 25 g of powders in each bottle. Afterwards, the powders were pressed in a disk template with 3 in diameter at 2500 psi for 30 s to make the multi-element target. For Pt deposition, four pieces (1×1 cm^2) of Pt foil (99.9 wt %) in 0.5 mm thickness were used. They were placed on the corners of the pre-pressed multi-element target and compressed at 5500 psi for 30 min at room temperature. In addition, a SiO_2 substrate (1×1 cm^2) was used as the reference and it was positioned near the noncatalyzed GDE during the sputter deposition. The chamber pressure was maintained below 5×10^{-6} Torr with a cryogenic pump. The target material was sputtered by Ar ions with a RF power supply of 100 W at 10 mTorr and the deposition of multi-element nanoparticles was taking place on the rotating noncatalyzed GDE and SiO_2 substrates. The distance of the target material to the substrates was 10 cm. The rotation speed of the substrates was 2 rpm. The substrate was not heated during the sputter deposition. The schematic of the sputter deposition setup is shown in Fig. 1.

Phase identification for the multi-element nanoparticles was conducted using a Siemens D5000 X-ray diffractometer (XRD) with Cu Kα radiation ($\lambda = 1.5418$ Å). A thermal field emission scanning electron microscope (SEM; JSM-6500F) was used to observe the morphologies of the multi-element nanoparticles on the noncatalyzed GDEs. Composition analysis was carried out by energy dispersive X-ray spectroscope (EDS) on films deposited on the SiO_2 substrates. The thickness of the deposited film was determined by a α stepper (Dektak 3ST). Cyclic voltammogram (CV) was recorded with a Solartron SI 1287 Potentiostat with 500 ml electrolyte containing 0.5 M H_2SO_4 and 1 M CH_3OH. The electrolyte was purged with nitrogen for 15 min and the measurement was postponed for 30 min allowing stabilization of the open circuit voltage. The GDE catalyzed by multi-element nanoparticles (electrode area ~ 0.87 cm^2) was used as the working electrode. The GDE was in contact with a stainless steel disk where an external lead was established to the potentiostat. The Ag/AgCl was used as the reference electrode, and the Pt foil was used as the counter electrode. The CVs and mass activity measurements were conducted in a range of 0–0.95 V vs the reference electrode at a scan rate 50 mV/s. All the electrochemical analysis was carried out at temperatures of 22–25 °C.

3. Results and Discussion

3.1 Electrocatalyst preparations

Due to variations in the sputtering yield, the molar ratio of Fe, Co, Ni, Cu, Ag, and the amount of Pt were adjusted several times to render nanoparticles with the desirable composition. Table I lists properties of the deposited films on the SiO_2 substrates with deposition times of 30, 40, and

Table I. Properties of the as-deposited multi-element films at various deposition times.

Sputtering time (min)	Atomic composition[a)]	Film thickness[b)] (nm)	Loading of electrocatalysts[c)] (mg/cm^2)	Density (g/cm^3)
30	$Pt_{50}Fe_{10}Co_9Ni_{11}Cu_{12}Ag_8$	159	0.248	15.6
40	$Pt_{51}Fe_{11}Co_{10}Ni_{10}Cu_{10}Ag_8$	217	0.331	15.3
120	$Pt_{50}Fe_{11}Co_{10}Ni_{11}Cu_{10}Ag_8$	656	0.993	15.4

a) from EDS
b) from α stepper
c) from calculation

120 min, respectively. As clearly presented, the atomic compositions of the as-deposited films were close to our target of $Pt_{50}Fe_{10}Co_{10}Ni_{10}Cu_{10}Ag_{10}$. In addition, the thickness and weight of the deposited films were found to increase with the deposition time. The deposition rate is calculated at 5.2 nm/min. Since the substrate area and thickness were known, we determined the catalyst loading by multiplying the theoretic density (derived from X-ray) with the total deposited volume. It is because direct weighting of the catalysts is nearly impossible as only a thin layer of nanoparticles was deposited on the GDE surface.

Figure 2 exhibits the XRD patterns of $Pt_{50}Fe_{11}Co_{10}Ni_{11}Cu_{10}Ag_8$ on the substrates of noncatalyzed GDE and SiO_2 after deposition of 120 min. The diffraction peaks from the SiO_2 substrate clearly indicated a well-crystalline fcc phase

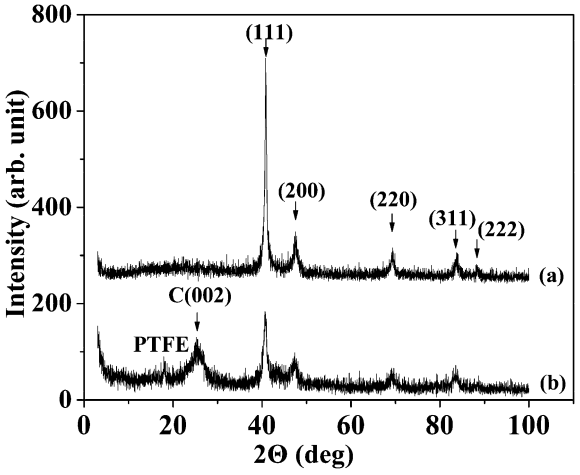

Fig. 2. XRD patterns of the multi-element $Pt_{50}Fe_{11}Co_{10}Ni_{11}Cu_{10}Ag_8$ films on the substrates of (a) SiO_2 and (b) noncatalyzed GDE. The deposition time is 120 min.

with relevant planes properly indexed. In contrast, moderate background noises were evident from the noncatalyzed GDE, which are attributed to the interferences from the carbon cloth and PTFE. The peaks at 18.1 and 25.2° were clearly from the PTFE and carbon (002), while remaining ones appeared identical to those from the SiO_2 substrate. Calculation of the lattice parameter using high-angle diffraction peaks arrives at 3.827 Å, which is a slight reduction from that of fcc Pt (3.923 Å). Because the atomic radii of Fe, Co, Ni, and Cu are considerably smaller than that of Pt, the lattice parameter of $Pt_{50}Fe_{11}Co_{10}Ni_{11}Cu_{10}Ag_8$ is expected to be reduced when a solid solution is formed following Vegard's law. Table II lists the characteristics of elements and analysis results of the $Pt_{50}Fe_{11}Co_{10}Ni_{11}Cu_{10}Ag_8$ films.

Figure 3 demonstrates the high-magnification SEM images of the noncatalyzed GDE as well as the GDEs after the sputter deposition of 1, 3, and 7 min, respectively. As shown in Fig. 3(a), the noncatalyzed GDE exhibited carbon particles in irregular shape approximately 50 nm in size. After deposition of 1 min shown in Fig. 3(b), there were subtle changes in the surface morphologies as the size of carbon particles increased slightly. After 3 min of deposition shown in Fig. 3(c), small nodules appeared on the surfaces of carbon particles with their average size increasing to 70 nm. The growth of nodules was uniform for all carbon particles. As shown in Fig. 3(d), further increase in the deposition time produced coarser particles with larger nodules on the surface. At this stage, the average diameter of carbon particles became 80 nm. In addition, preliminary phase of nodule coalescence was apparent. These results indicate a distinct morphological evolution that is consistent with the calculated deposition rate of 5.2 nm/min. Direct analysis of XRD on these multi-element nanoparticles is unavailable. However, because a crystalline fcc phase was identified by XRD for the sample with 2 h of deposition, and annealing treatment was not employed in our experiments, it is likely that each nodule on the carbon particle is a crystalline fcc grain.

3.2 Electrochemical characterizations

The objective of our investigation is to fabricate multi-element electrocatalysts on the noncatalyzed GDEs for the methanol oxidation in DMFC. Therefore, we focus our activities in analyzing the electrochemical performances of samples with deposition times of 1, 3, and 7 min. They correspond to electrocatalyst loadings of 0.008 mg/cm^2 (5.2 nm), 0.025 mg/cm^2 (15.6 nm), and 0.058 mg/cm^2 (36.4 nm), respectively. Figure 4 presents the CV responses at various

Table II. Characteristics of the elements used in preparation for the multi-element nanoparticles and the as-deposited $Pt_{50}Fe_{11}Co_{10}Ni_{11}Cu_{10}Ag_8$ films.

	Element						Composition
	Fe[a)]	Co[a)]	Ni[a)]	Cu[a)]	Ag[a)]	Pt[a)]	$Pt_{50}Fe_{11}Co_{10}Ni_{11}Cu_{10}Ag_8$[b)]
Atomic weight	55.9	58.9	58.7	63.6	108	195	133.9
Atomic radius (Å)	1.24	1.25	1.25	1.28	1.44	1.38	1.35[c)]
Crystal structure	bcc	hcp	fcc	fcc	fcc	fcc	fcc[c)]

a) from ref. 25
b) from EDS
c) from XRD

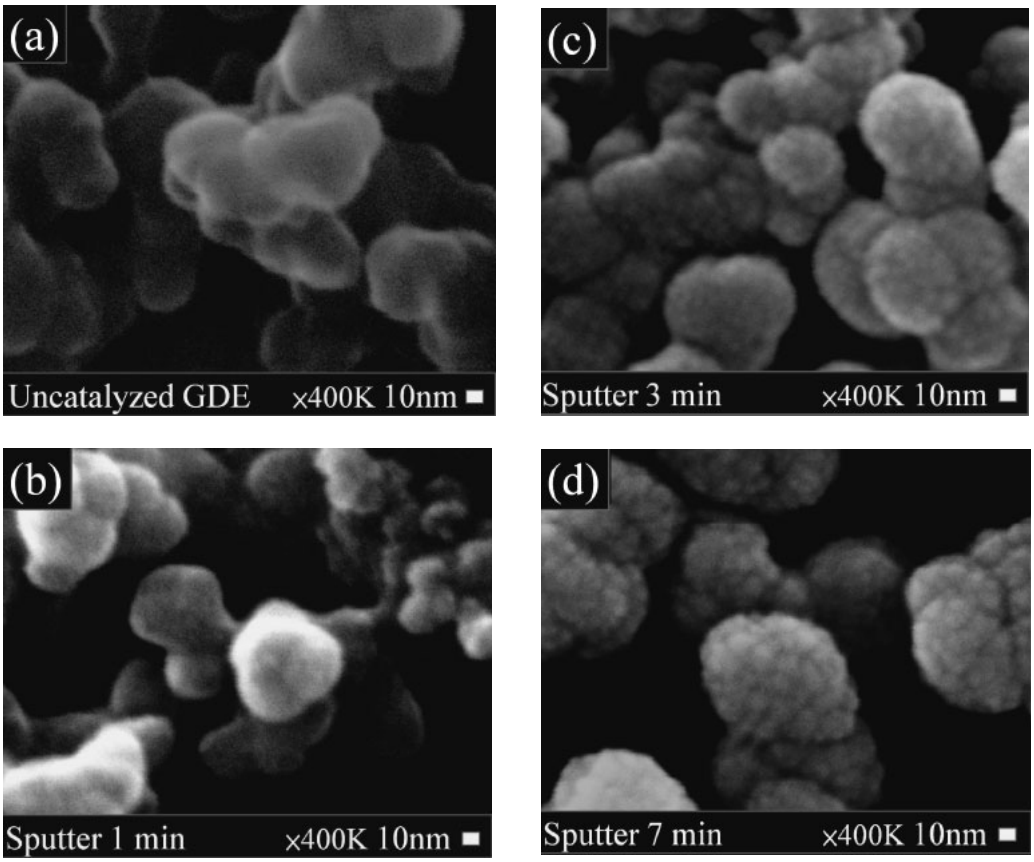

Fig. 3. SEM images of the (a) noncatalyzed GDE and $Pt_{50}Fe_{11}Co_{10}Ni_{11}Cu_{10}Ag_8$ catalyzed GDEs at deposition times of (b) 1, (c) 3, and (d) 7 min, respectively.

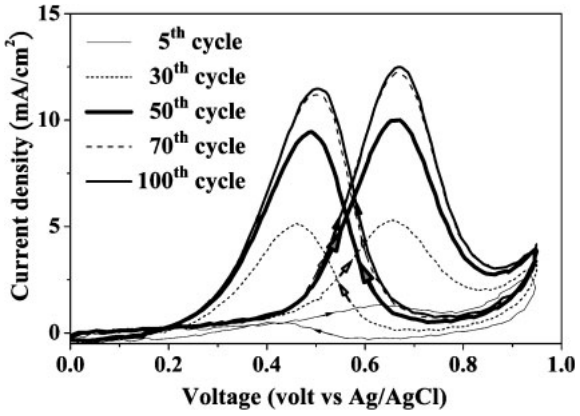

Fig. 4. CV curves of the $Pt_{50}Fe_{11}Co_{10}Ni_{11}Cu_{10}Ag_8$ catalyzed GDEs at the 5th, 30th, 50th, 70th, and 100th cycle, respectively. The deposition time is 3 min.

Table III. The electrochemical parameters from the CV scans at various cycles on the multi-element nanoparticles deposited for 3 min.

Cycle	Anodic scan		Cathodic scan		i_a/i_c
	V_a a) (V)	i_a b) (mA/cm^2)	V_c c) (V)	i_c d) (mA/cm^2)	
5th	0.635	1.333	0.416	0.474	N/A
30th	0.652	5.290	0.465	5.066	1.04
50th	0.671	9.995	0.491	9.449	1.06
70th	0.668	12.253	0.500	11.192	1.09
100th	0.668	12.498	0.501	11.475	1.09

a) potential at peak current density in anodic scan
b) peak current density in anodic scan
c) potential at peak current density in cathodic scan
d) peak current density in cathodic scan

cycles from the GDE after 3 min of deposition. As clearly shown, the CV curves improved gradually upon cycling. At the fifth cycle, the catalyzed GDE revealed limited current outputs. However, continued cycling was found to enhance its performance with the emergence of two distinct humps after the 30th cycle. The improvements in CV response became stabilized after the 70th cycle and there was negligible difference between the 70th and 100th cycle. Table III provides the details of electrochemical parameters from these CV scans. From the literature, the anodic peak is responsible for the oxidation of methanol while the cathodic peak corresponds to the oxidation of carbonaceous species produced from earlier methanol oxidation.[26] The values of V_a and V_c stand for the voltages at anodic and cathodic peaks, respectively. The i_a is the peak current in the anodic scan while the i_c represents the peak current in the cathodic scan. As reported previously, the ratio of i_a/i_c indicates the electrocatalytic ability to remove CO.[27,28] Hence, a higher ratio of i_a/i_c is always preferred. In our case, the values for i_a/i_c remain relatively constant between 1.04–1.09. This implies that the atoms responsible for the catalytic reaction are possibly unchanged upon cycling. On the other hand, the values for V_a and V_c are moving to positive potentials, suggesting gradual deterioration in catalytic performances, a behavior associated with catalyst poisoning.

The evolution of CV responses upon cycling is not uncommon. Typically it is recognized as the "electrochemical annealing" whereas the surface rearrangement of catalytic atoms and preferential adsorption of particular ions are likely responsible. However, the nature of "electrochemical annealing" varies contingent on specific systems involved. For example, Cao *et al.* reported improving CV behaviors upon cycling and they attributed their observations to the reduced activation of $RuO_2 \cdot 0.56H_2O$.[29] In contrast, Uchida *et al.* noted deteriorations of CV upon cycling for the PtFe and inferred dissolution of Fe as the likely cause.[7] In our case the steady increase in current upon CV cycling is possibly due to the preferential dissolutions of Fe, Co, Ni, Cu, and Ag, resulting in a large portion of Pt on the GDE surface. The anodic dissolution of those elements is expected because the acidic electrolyte involved as well as the anodic potential imposed in the CV scans. Practices of "preferential dissolution" in the PtCuCo to fabricate a Pt-rich surface layer for enhanced catalytic abilities were reported recently by Strivastava *et al.*,[30] as well as Koh and Strasser.[31] Our results are consistent with their reports in which excess Pt was present on the surface of electrocatalysts. Unfortunately, the predominant Pt of the multi-element nanoparticles was poisoned rapidly, confirming the constant i_a/i_c upon CV cycling.

Figure 5 exhibits the SEM images of the multi-element nanoparticles before and after CV scans of 100 cycles. After 100 cycles, it is noted that the nanoparticles were slightly smaller with disappearance of characteristic surface nodules. In addition, EDS analysis of the composition revealed partial decreases of Fe, Co, Ni, and Cu. Unfortunately, quantitative determination of the exact loss is unavailable because of the strong background interferences from carbon.

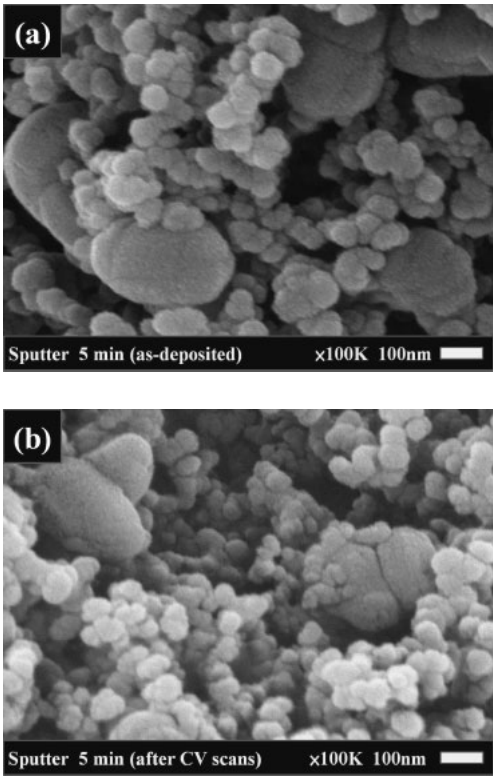

Fig. 5. SEM images of the $Pt_{50}Fe_{11}Co_{10}Ni_{11}Cu_{10}Ag_8$ catalyzed GDEs (a) before and (b) after CV scan of 100 cycles.

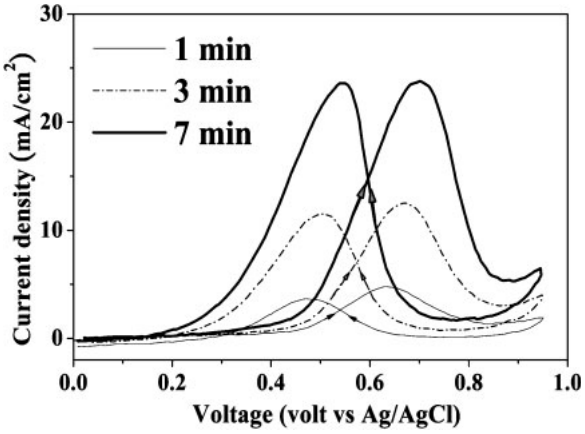

Fig. 6. CV curves of the $Pt_{50}Fe_{11}Co_{10}Ni_{11}Cu_{10}Ag_8$ catalyzed GDEs at the 100th cycle with deposition times of 1, 3, and 7 min, respectively.

To remove the influence of the anodic dissolution in surface atoms, the CV scan of the 100th cycle was selected as the indicator of catalytic abilities in our study. Figure 6 exhibits the results for the GDEs with deposition times of 1, 3, and 7 min, respectively. During the anodic scan, the peak potentials of 1, 3, and 7 min were located at 0.638, 0.668, and 0.701 V, respectively. Likewise, the peak potentials from the cathodic scan of 1, 3, and 7 min were identified at 0.474, 0.501, and 0.550 V, respectively. For both anodic and cathodic peaks, their values increased with the deposition time. In addition, the onset potentials for the methanol oxidation were determined at 0.267, 0.228, and 0.210 V for 1, 3, and 7 min, respectively. Because the loadings of electrocatalyst were estimated at 0.008, 0.025, and 0.058 mg/cm^2 for the samples of 1, 3, and 7 min, the peak current and area under the CV curves were proportional to the loadings of the electrocatalyst as expected. Table IV provides the electrochemical parameters from these CV scans. As clearly presented, the value for i_a/i_c reaches as high as 1.33 for the sample deposited for 1 min. With extended deposition time, the value of i_a/i_c drops considerably to a value of 1.01.

Because the deposition time directly determines the exact amount of nanoparticles on the GDEs, true catalytic performances of electrocatalysts can only be analyzed by comparing their mass activity (mA/mg). These data were normalized by the overall catalyst loadings to represent the intrinsic catalytic abilities for methanol oxidation. Figure 7

Table IV. The electrochemical parameters from CV scans of the 100th cycle on the multi-element nanoparticles deposited for 1, 3, and 7 min, respectively.

Time (min)	Anodic scan		Cathodic scan		i_a/i_c
	V_a [a] (V)	i_a [b] (mA/cm^2)	V_c [c] (V)	i_c [d] (mA/cm^2)	
1	0.638	4.793	0.474	3.613	1.33
3	0.668	12.498	0.501	11.475	1.09
7	0.701	23.768	0.550	23.605	1.01

a) potential at peak current density in anodic scan
b) peak current density in anodic scan
c) potential at peak current density in cathodic scan
d) peak current density in cathodic scan

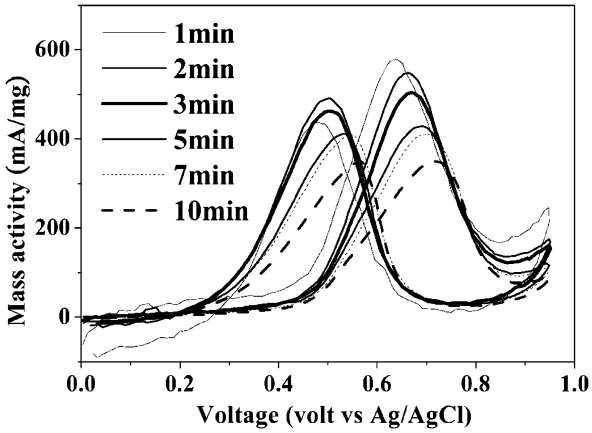

Fig. 7. Mass activities of the $Pt_{50}Fe_{11}Co_{10}Ni_{11}Cu_{10}Ag_8$ catalyzed GDEs at the 100th cycle with deposition times of 1, 2, 3, 5, 7, and 10 min, respectively.

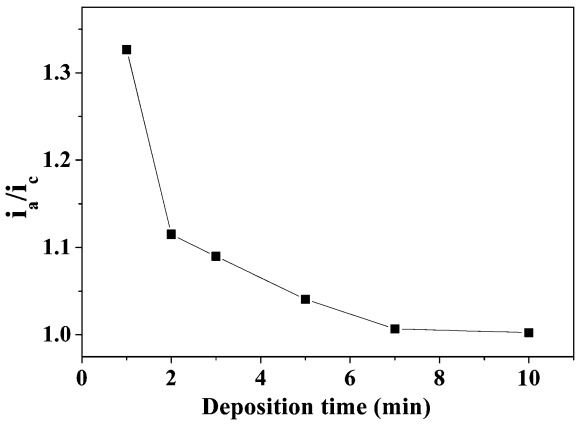

Fig. 8. The values for i_a/i_c for the catalyzed GDEs at the 100th cycle with depoistion times of 1, 2, 3, 5, 7, and 10 min, respectively.

demonstrates the CV responses of the mass activities for the GDEs at the 100th cycle with deposition times of 1, 2, 3, 5, 7, and 10 min, respectively. They correspond to nanoparticles with diameters between 5–52 nm and catalyst loadings of 0.0083–0.083 mg/cm^2. As clearly shown, the mass activities revealed by the nanoparticles of 1 min deposition demonstrated the strongest ability, with values reaching as high as 400–500 mA/mg. In addition, the mass activities were found to decrease orderly with increasing deposition time, indicating nanoparticles of larger size is undesirable for catalytic performances. Furthermore, the peak current from the anodic scan moved to more positive potentials with increasing deposition time. These results suggest the morphologies of the multi-element nanoparticles play substantial roles over the resulting electrochemical behaviors. The values of mass activity measured here (400–600 mA/mg) are in agreement with what were reported earlier by Gu and Wong,[32] as well as Prabhuram *et al.*[33] Figure 8 presents the values of i_a/i_c for the GDEs after deposition of 1, 2, 3, 5, 7, and 10 min, respectively. Analysis of the i_a/i_c in our samples reveals a decreasing trend for increasing deposition time, indicating the smallest particles (~5 nm) possess the highest abilities.

Similar sputtering procedures were conducted to prepare the GDEs decorated with nanoparticulate Pt and $Pt_{43}Ru_{57}$.

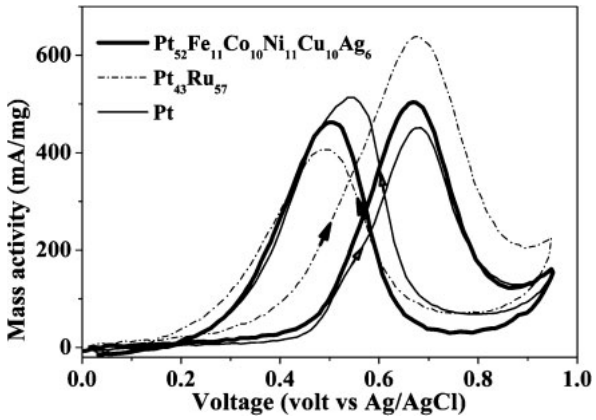

Fig. 9. Mass activities of the GDEs catalyzed by 3 min deposition of the Pt, $Pt_{43}Ru_{57}$, and $Pt_{50}Fe_{11}Co_{10}Ni_{11}Cu_{10}Ag_8$, respectively. The deposition time is 3 min and the data were recorded at the 100th cycle.

Table V. The electrochemical parameters from the CV scan on the GDEs catalyzed by the Pt, $Pt_{43}Ru_{57}$, and $Pt_{50}Fe_{11}Co_{10}Ni_{11}Cu_{10}Ag_8$ at the 100th cycle. The deposition time is 3 min.

Catalyst	Anodic scan		Cathodic scan		i_a/i_c
	V_a[a] (V)	i_a[b] (mA/cm^2)	V_c[c] (V)	i_c[d] (mA/cm^2)	
Pt	0.684	451	0.549	513	0.88
$Pt_{43}Ru_{57}$	0.677	638	0.486	406	1.57
$Pt_{50}Fe_{11}Co_{10}Ni_{11}Cu_{10}Ag_8$	0.668	504	0.501	462	1.09

a) potential at peak current density in anodic scan
b) peak current density in anodic scan
c) potential at peak current density in cathodic scan
d) peak current density in cathodic scan

The deposition rates for the Pt and $Pt_{43}Ru_{57}$ are 6.3 nm/min (0.014 mg min^{-1} cm^{-2}) and 4.6 nm/min (0.007 mg min^{-1} cm^{-2}), respectively. The mass activities from the CV scans at the 100th cycle of the catalyzed GDEs after 3 min deposition were used for comparison and their results are demonstrated in Fig. 9. The catalyst loadings for the Pt and $Pt_{43}Ru_{57}$ were 0.036 and 0.018 mg/cm^2, respectively. Relevant electrochemical parameters are also listed in Table V. As clearly shown, the mass activities for the $Pt_{43}Ru_{57}$ exhibited the highest performance, reaching values as high as 638 mA/mg. In contrast, the mass activities for the Pt revealed the poorest behavior at a moderate value of 451 mA/mg. In addition, the area under the CV response for the $Pt_{43}Ru_{57}$ was significantly larger than those of Pt and $Pt_{50}Fe_{11}Co_{10}Ni_{11}Cu_{10}Ag_8$. The onset potentials for the Pt, $Pt_{43}Ru_{57}$, and $Pt_{50}Fe_{11}Co_{10}Ni_{11}Cu_{10}Ag_8$ were 0.188, 0.089, and 0.228 V, respectively. Furthermore, the values for i_a/i_c are 0.88, 1.57, and 1.09, respectively. These results confirm the superiority of $Pt_{43}Ru_{57}$, a fact which is well-established in literatures. Despite the multi-element nanoparticles can not deliver comparable performances to those of $Pt_{43}Ru_{57}$, its behaviors still demonstrated notable improvements over those of Pt.

An alloy with multiple principal elements is known as the high-entropy alloy. Preliminary analysis on the possible high-entropy effect to the $Pt_{50}Fe_{11}Co_{10}Ni_{11}Cu_{10}Ag_8$ nanoparticles is necessary. Basing on the definition of high-

entropy alloy proposed by Yeh *et al.*,[15] constituent elements must be equimolar or near-equimolar. Thus, following Boltzmann's hypothesis the configurational entropy change of an equimolar alloy with six elements can be calculated by

$$\Delta S_{\text{conf}} = -k \ln \omega = -R \sum \frac{1}{n} \ln\left(\frac{1}{n}\right) = R \ln n = 1.792R \ (\text{J K}^{-1}\,\text{mole}^{-1}) \quad (1)$$

In our multi-element nanoparticles, the molar ratio of Pt : Fe : Co : Ni : Cu : Ag is close to 5 : 1 : 1 : 1 : 1 : 1. As a result, the configurational entropy change of alloying is estimated at

$$\Delta S_{\text{conf}} = -R\left[\frac{1}{2}\ln\left(\frac{1}{2}\right) + 5 \times \frac{1}{10}\ln\left(\frac{1}{10}\right)\right] = 1.498R \ (\text{J K}^{-1}\,\text{mole}^{-1}). \quad (2)$$

Similarly, the entropy change for the Pt and $Pt_{43}Ru_{57}$ are $0R$ and $0.683R$, respectively. Although the value of $1.498R$ is slightly below than the $1.792R$ of equimolar high-entropy system, it is possible that the moderate increase in entropy contributes to the observed catalytic enhancement over that of Pt. Our results of electrochemical characterization provide preliminary information on the multi-element nanoparticles for potential application as electrocatalysts. Despite lack of significant enhancements in the catalytic behaviors to compete with the $Pt_{43}Ru_{57}$, notable improvements over those of Pt were observed. Further investigations are currently underway to prepare the samples with deliberately controlled surface morphologies for better catalytic characteristics.

4. Conclusions

Depositions of multi-element nanoparticles on the non-catalyzed GDEs were conducted by radio frequency sputtering. XRD analysis of the as-deposited films exhibited crystalline fcc phases while EDS confirmed their composition as $Pt_{50}Fe_{11}Co_{10}Ni_{11}Cu_{10}Ag_8$. With a deposition rate of 5.2 nm/min, the sputtering process lasted for 1, 2, 3, 5, 7, and 10 min to prepare a thin layer of multi-element nanoparticles on the GDE surface for electrochemical characterizations. From SEM images, the multi-element nanoparticles appeared as nodules grown on the carbon particles. The CV responses of the catalyzed GDEs increased upon cycling and became stabilized after the 70th cycle. The CV results of GDEs at the 100th cycle revealed an increase of performance with deposition time. In mass activities, the samples with 1 min deposition demonstrated the highest values. In comparison with the Pt and $Pt_{43}Ru_{57}$, the $Pt_{50}Fe_{11}Co_{10}Ni_{11}Cu_{10}Ag_8$ demonstrated better catalytic ability than that of Pt but its performance was still below to that of $Pt_{43}Ru_{57}$.

Acknowledgements

The authors would like to thank the National Science Council of R.O.C. for financial support under the contract of NSC96-2221-E-009-110. Equipment assistances from Professor Chiun-Hsun Chen of Mechanical Engineering Department are highly appreciated.

1) B. C. H. Steele and A. Heinzel: Nature **414** (2001) 345.
2) M. P. Hogarth and T. R. Ralph: Platinum Met. Rev. **46** (2002) 146.
3) H. Liu, C. Song, L. Zhang, J. Zhang, H. Wang, and D. P. Wilkinson: J. Power Sources **155** (2006) 95.
4) T. Yajima, H. Uchida, and M. Watanabe: J. Phys. Chem. B **108** (2004) 2654.
5) P. Waszczuk, G. Q. Lu, A. Wieckowski, C. Lu, C. Rice, and R. I. Masel: Electrochim. Acta **47** (2002) 3637.
6) X. Li and I. M. Hsing: Electrochim. Acta **52** (2006) 1358.
7) H. Uchida, H. Ozuka, and M. Watanabe: Electrochim. Acta **47** (2002) 3629.
8) H. Igarashi, T. Fujino, Y. Zhu, H. Uchida, and M. Watanabe: Phys. Chem. Chem. Phys. **3** (2001) 306.
9) E. Antolini, J. R. C. Salgado, A. M. dos Santos, and E. R. Gonzalez: Electrochem. Solid-State Lett. **8** (2005) A226.
10) P. Strasser, Q. Fan, M. Devenney, W. H. Weinberg, P. Liu, and J. K. Nørskov: J. Phys. Chem. B **107** (2003) 11013.
11) B. Gurau, R. Viswanathan, R. Liu, T. J. Lafrenz, K. L. Ley, E. S. Smotkin, E. Reddington, A. Sapienza, B. C. Chan, T. E. Mallouk, and S. Sarangapani: J. Phys. Chem. B **102** (1998) 9997.
12) E. Reddington, A. Sapienza, B. Gurau, R. Viswanathan, S. Sarangapani, E. S. Smotkin, and T. Mallouk: Science **280** (1998) 1735.
13) J. F. Whitacre, T. Valdez, and S. R. Narayanan: J. Electrochem. Soc. **152** (2005) A1780.
14) K. W. Park, J. H. Choi, S. A. Lee, C. Pak, H. Chang, and Y. E. Sung: J. Catal. **224** (2004) 236.
15) J. W. Yeh, S. K. Chen, S. J. Lin, J. Y. Gan, T. S. Chin, T. T. Shun, C. H. Tsau, and S. Y. Chang: Adv. Eng. Mater. **6** (2004) 299.
16) Y. Y. Chen, U. T. Hong, J. W. Yeh, and H. C. Shih: Appl. Phys. Lett. **87** (2005) 261918.
17) Y.-S. Huang, L. Chen, H.-W. Lui, M.-H. Cai, and J.-W. Yeh: Mater. Sci. Eng. A **457** (2007) 77.
18) C. Y. Hsu, J. W. Yeh, S. K. Chen, and T. T. Shun: Metall. Mater. Trans. A **35** (2004) 1465.
19) R. O'Hayre, S.-J. Lee, S.-W. Cha, and F. B. Prinz: J. Power Sources **109** (2002) 483.
20) A. T. Haug, R. E. White, J. W. Weidner, W. Huang, S. Shi, T. Stoner, and N. Rana: J. Electrochem. Soc. **149** (2002) A280.
21) M. Alvisi, G. Galtieri, L. Giorgi, R. Giorgi, E. Serra, and M. A. Signore: Surf. Coat. Technol. **200** (2005) 1325.
22) T. K. Chen, M. S. Wong, T. T. Shun, and J. W. Yeh: Surf. Coat. Technol. **200** (2005) 1361.
23) T. Page, R. Johnson, J. Hormes, S. Noding, and B. Rambabu: J. Electroanal. Chem. **485** (2000) 34.
24) S. Martínez and C. F. Zinola: J. Solid State Electrochem. **11** (2007) 947.
25) J. Emsley: *The Elements* (Oxford University Press, Oxford, U.K., 1991) 2nd ed., p. 10.
26) Y. J. Gu and W. T. Wong: Langmuir **22** (2006) 11447.
27) M. C. Tsai, T. K. Yeh, and C. H. Tsai: Electrochem. Commun. **8** (2006) 1445.
28) J. Bagchi and S. K. Bhattacharya: J. Power Sources **163** (2007) 661.
29) L. Cao, F. Scheiba, C. Roth, F. Schweiger, C. Cremers, U. Stimming, H. Fuess, L. Chen, W. Zhu, and X. Qiu: Angew. Chem., Int. Ed. **45** (2006) 5315.
30) R. Srivastava, P. Mani, N. Hahn, and P. Strasser: Angew. Chem., Int. Ed. **46** (2007) 8988.
31) S. Koh and P. Strasser: J. Am. Chem. Soc. **129** (2007) 12624.
32) Y. J. Gu and W. T. Wong: J. Electrochem. Soc. **153** (2006) A1714.
33) J. Prabhuram, T. S. Zhao, Z. X. Liang, and R. Chen: Electrochim. Acta **52** (2007) 2649.